IEEE Access
Multidisciplinary ⋮ Rapid Review ⋮ Open Access Journal

Received 19 January 2023, accepted 17 February 2023, date of publication 24 February 2023, date of current version 14 March 2023.

Digital Object Identifier 10.1109/ACCESS.2023.3249107

RESEARCH ARTICLE

Two-Switch Boost Converter With Improved Voltage Gain and Degree of Freedom of Control

R. V. DAMODARAN[1], HUSSAIN SHAREEF[1,2], (Member, IEEE), K. S. PHANI KIRANMAI[1], AND RACHID ERROUISSI[1], (Senior Member, IEEE)

[1]Department of Electrical and Communication Engineering, United Arab Emirates University, Al Ain, United Arab Emirates
[2]National Water and Energy Center, United Arab Emirates University, Al Ain, United Arab Emirates

Corresponding author: Hussain Shareef (shareef@uaeu.ac.ae)

This work was supported by the Asian Universities Alliance (AUA)–United Arab Emirates University Joint Research Program (project title: ''High Power Density AC Solar Module for Maximum Energy Yield With Real-Time Monitoring and Intelligent Fault Detection Capabilities'') under Grant G00004215.

ABSTRACT The use of renewable resources for low power generation has led to extensive research on power converters for reliable and efficient power conversion. Though conventional boost converter (CBC) remains the widely used topology, its operating range is limited due to constraints on voltage gain and degree of freedom of control (DoFoC). This paper presents a two-switch boost converter (TSBC) which improves the voltage gain and DoFoC by cascading an additional switch-diode pair to the CBC circuit. The additional switch enhances the range of voltage gain without operating CBC at high duty ratios. Additionally, TSBC offers more choices to adjust voltage gain, which enhances DoFoC. The switching interval selection is detailed considering the voltage gain and constraints on circuit variables. The design formulations of TSBC are examined to facilitate optimal choice of components. The features of TSBC are theoretically established with mathematical derivations and are validated by simulations and experiments. The experimental results indicate that for a duty ratio of 0.7 for the existing switch of CBC, an increase in voltage gain from 3.2 to 4.3 is achieved when the duty ratio of the additional switch in TSBC is varied from 0 to 0.1. Similarly, improved DoFoC is demonstrated with inductor current control as well as with constant ripple ratios while maintaining the required output voltage. The proposed converter can easily replace the commonly CBC to improve the gain and DoFoC by simply cascading a switch-diode pair at the input-side of CBC.

INDEX TERMS Boost converter, cascaded topology, degree of freedom, voltage gain, ripple ratio.

I. INTRODUCTION

Renewable resources and energy storage systems such as solar photo-voltaic (PV), wind turbines, fuel cells, and battery storage have steadily gained acceptance as dependable and low-cost means of fulfilling the ever-increasing energy demand. As a result, the number of non-conventional sources integrated into the existing distribution system has extensively increased over the past few decades. This escalating use of renewable resources along with the advancement in the area of semiconductor devices and the competitive energy market has influenced the research on power converter interfaces (PCIs) [1], [2]. PCIs are primarily ought to have a simple structure with small size and high efficiency [3]. To achieve safe, stable, cost-effective, and reliable integration, developing converters that comply with updated standards and achieve increased efficiency is critical.

Several existing low-power renewable resources have high power to voltage ratio and therefore require a voltage boosting stage [4], [5]. The conventional boost converter (CBC) is most commonly used for this purpose due to its simple circuit and available comprehensive analysis [2]. However, CBC exhibits several inadequacies in many applications, one of which is the constraint on its practical voltage gain. Although CBC theoretically yields significant voltage gains, it is practically unattainable due to parasitic resistances, stresses on

The associate editor coordinating the review of this manuscript and approving it for publication was Chi-Seng Lam.

switching devices, as well as stability and efficiency concerns at high duty ratios. This limit on voltage gain can lead to over-sizing of the sources [6], [7]. To this end, several step-up converters have been proposed in the existing literature.

The topologies for step-up DC–DC converters can be categorized as isolated and non-isolated converters [8]. Isolated converters use traditional or multi-winding transformers to achieve the necessary voltage gain and maintain isolation between input and output sides [9], [10], [11], [12]. The existence of a transformer, on the other hand, necessitates a high-frequency stage and increases the total loss. Due to low cost, size, and efficiency, non-isolated converters are frequently preferred in low-power systems [6]. Many existing non-isolated converters achieve high voltage gain ratios by increasing the voltage multiplier cells [4], [5], using coupled inductors with high turns ratios or with switched capacitor [13], [14] or inductor modules [15], [16], [17]. Though transformer-based or coupled-inductor-based high-gain converters have several advantages, the presence of magnetic elements with strict design constraints degrades its structural simplicity [10], [18]. The switched capacitor and inductor converters, on the other hand, necessitate a large number of high-frequency switching devices and suffer from excessive current and voltage spikes during transients [13]. Another method to attain high voltage gain is with cascaded converters [19], [20]. If integrated with careful design of components, the cascading technique can be used to develop converters with improved voltage gains.

Another restriction of CBC is the lack of diverse degrees of freedom of control (DoFoC) under continuous conduction mode (CCM). This implies the duty ratio is varied to control only one variable. Due to this, the CBC is designed at the rated maximum operating conditions which results in over-sizing of the converter. This initiated the development of converters with higher DoFoC. High gain converters based on coupled-inductor impedance sources depend on the inductor turns ratio and coupling to increase DoFoC [21], [22], [23], [24]. In [25], a boost converter with interleaved inductor and switched capacitor voltage multiplier to eliminate input current ripple at a pre-selected duty ratio is presented. However, pre-selection of duty ratio may not be feasible in many applications. A soft-switching boost converter with unidirectional cell to increase DoFoC and efficiency is proposed in [18]. However, its voltage gain require further analysis and comparison. Several high-gain converters in literature achieve higher DoFoC with complex circuit or control strategies. Contrarily, cascaded converter configurations resolve the constraint on DoFoC and attain increased voltage gains.

Considering the above-mentioned factors as motivation, a two-switch boost converter (TSBC) is proposed in this paper to improve the voltage gain of CBC by cascading a switch-diode pair. The inclusion of extra switch increases the DoFoC in comparison to CBC. The proposed TSBC circuit is easy to implement by including a switch-diode pair to CBC in case of an existing PCI or by using two half-bridges in a new system. The significant contributions of the paper are as follows.

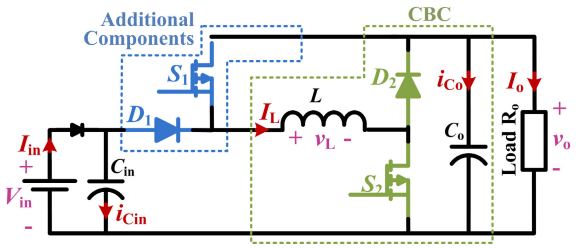

FIGURE 1. Circuit of the proposed TSBC.

- A novel TSBC with improved voltage gain with minimal circuit changes to CBC
- Analysis to apprehend the increased DoFoC due to the inclusion of the additional switch
- A meticulous switching interval selection to provide ease of control implementation
- A detailed formulation for component sizing of the proposed TSBC to facilitate simple hardware development

The rest of the paper is organized as follows. Section II discusses the proposed TSBC circuit and analyzes it during different states of operation to derive Important formulations including the voltage gain and current relations. The increased DoFoC due to the availability of multiple switching combinations is explained in section III. In section IV, the improvement in voltage gain of the proposed TSBC in comparison to CBC is presented. The selection of duty ratios considering constraints on different variables is discussed in section V. Section VI contains formulations for optimal component sizing, followed by a comparison of specifications for the proposed TSBC and CBC. The simulation and experimental findings are reported in section VII to validate the theoretical claims of improved voltage gain and DoFoC. The conclusions from the theoretical analysis and results are finally summarized in section VIII.

II. CIRCUIT ANALYSIS OF PROPOSED CONVERTER

The circuit of the proposed TSBC is shown in Fig. 1 with an input voltage V_{in} and output voltage V_o across a load R_o. It consists of an input filter capacitor C_{in}, a pair of switches (S_1, S_2), a pair of diodes (D_1, D_2), an inductor L, and output capacitor C_o. The average input, output and inductor currents are denoted by I_{in}, I_o and I_L respectively. The switches can be operated synchronously or independently. The circuit implementation of TSBC is considered to be simple as it comprises of a switch and diode at the input side of CBC.

A. CIRCUIT ANALYSIS

Assuming CCM operation, diodes D_1 and D_2 conduct in complement to switches S_1 and S_2 respectively. Hence, there exist four states of operation based on switching conditions of S_1 and S_2 as shown in Table 1 and are discussed as follows.

TABLE 1. Switching states and corresponding variables.

State	S_2,S_1	Interval	v_L	$i_{C_{in}}$	i_{C_o}
0	OFF,OFF	t_0	$V_{in} - V_o$	$I_{in} - I_L$	$I_L - I_o$
1	OFF,ON	t_1	0	I_{in}	$-I_o$
2	ON,OFF	t_2	V_{in}	$I_{in} - I_L$	$-I_o$
3	ON,ON	t_3	V_o	I_{in}	$-I_L - I_o$

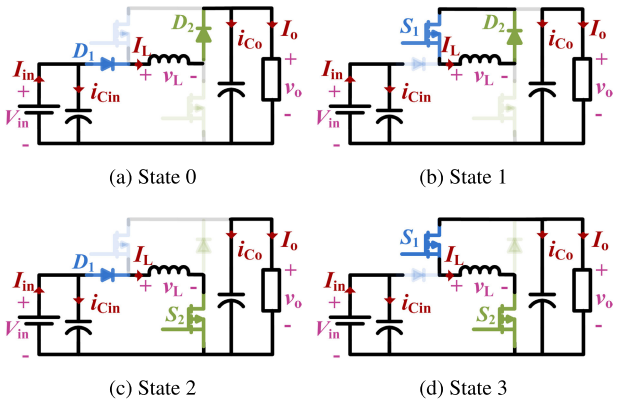

(a) State 0 (b) State 1

(c) State 2 (d) State 3

FIGURE 2. States of operation of the proposed TSBC.

1) STATE 0

The circuit operates in state 0 for the time interval t_0 when both the switches are OFF. If the inductor current i_L is non-zero, the diodes D_1 and D_2 conduct as shown in Fig. 2. The input source along with the inductor supply power to the load. The voltage and currents of energy storage elements are determined by circuit analysis as shown in (1).

$$[v_L, i_{C_o}, i_{C_{in}}] = [(V_{in} - V_o), (I_L - I_o), (I_{in} - I_L)] \quad (1)$$

2) STATE 1

During state 1, the switch S_1 is ON while S_2 is OFF as shown in Fig. 2b. The time interval for this state is t_1. The input source supplies the input capacitor C_{in} while the output capacitor C_o supplies the load. The inductor current i_L remains constant and circulates through S_1 and D_2. The following equations are obtained by circuit analysis of Fig. 2b.

$$[v_L, i_{C_o}, i_{C_{in}}] = [(0), (-I_o), (I_{in})] \quad (2)$$

State 2

The circuit operates in state 2 for t_2, during which the switch S_1 OFF while switch S_2 is ON. The inductor is charged from the input via the diode D_1 and switch S_2, while the load is supplied solely by the output capacitor C_o. The following equations are obtained for this state.

$$[v_L, i_{C_o}, i_{C_{in}}] = [(V_{in}), (-I_o), (I_{in} - I_L)] \quad (3)$$

State 3

Both switches S_1 and S_2 are ON for a interval of t_3 in state 3. The inductor L discharges to the output capacitor C_o and the load, while the capacitor C_{in} is sourced from the input. The equations that characterize this state are as follows.

$$[v_L, i_{C_o}, i_{C_{in}}] = [(V_o), (I_L - I_o), (I_{in})] \quad (4)$$

From the circuit analysis, the operation of TSBC in state 0 and state 2 are noted to be identical to that of CBC. Hence, the proposed TSBC operates as a CBC when switch S_1 remains off throughout the circuit operation.

B. VOLTAGE AND CURRENT RATIOS

If the passive components are assumed to be loss-less, the average energy dissipated across C_{in}, L and C_o during one switching period $T(= \sum_{i=0}^{3} t_i)$ can be equated to zero. From v_L in (1), (2), (3) and (4), the following relation can be derived considering zero energy dissipation in the inductor.

$$(V_{in} - V_o)t_0 + V_{in}t_2 + V_o t_3 = 0 \quad (5)$$

Therefore, the relation between the output and input voltages can be derived in terms of the switching intervals as

$$V_o = V_{in}\frac{t_0 + t_2}{t_0 - t_3} \quad ; \quad t_0 > t_3 \quad (6)$$

Similarly, by equating the average energy dissipated in the capacitors C_{in} and C_o to zero, we obtain (7) and (8).

$$(I_{in} - I_L)(t_0 + t_2) + I_{in}(t_1 + t_3) = 0 \quad (7)$$

$$(I_L - I_o)t_0 - I_o(t_1 + t_2) + (-I_L - I_o)t_3 = 0 \quad (8)$$

From (7) and (8), the relation between average currents in the circuit is derived an in (9).

$$I_L = I_o\frac{T}{t_0 - t_3} = I_{in}\frac{T}{t_0 + t_2} \quad (9)$$

It is observed from (6) and (9), there exist multiple combinations of time intervals t_{0-3} that yield the same voltage or current relation. This enables control of additional variables.

III. DUTY RATIOS AND OVERLAP OF SWITCH PULSES

Based on (6), different combinations of time intervals t_{0-3} can be used to achieve a required voltage ratio. For ease of control implementation, these time intervals are hereafter expressed in terms of the duty ratios of switching pulses and the ratio of their overlap. Let the duty ratios of the switching pulses to S_1 and S_2 be d_1 and d_2 respectively while their ratio of overlap time to time period T be d_{OL} as shown in Fig. 3. The duty ratios d_1 and d_2 and their overlap ratio can be expressed in terms of the intervals t_{0-3} as in (10).

$$\begin{bmatrix} d_1 \\ d_2 \\ d_{OL} \end{bmatrix} = \frac{1}{T}\begin{bmatrix} t_1 + t_3 \\ t_2 + t_3 \\ t_3 \end{bmatrix} \quad (10)$$

It is observed from (10) that for the same set of duty ratios (d_1, d_2), the time intervals t_{0-3} vary when overlap ratio d_{OL} is varied. From Fig. 3, d_{OL} can be varied by introducing a phase shift between the switching pulses S_1 and S_2. The phase shift

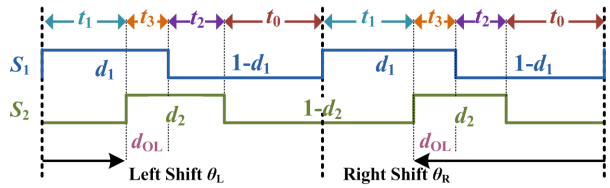

FIGURE 3. Switching pulses of S_1 and S_2 with overlap.

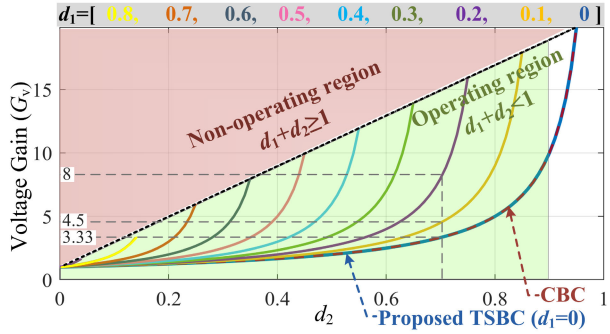

FIGURE 4. Voltage gain ratios for CBC and proposed TSBC.

θ_{OL} of S_2 w.r.t. S_1 in seconds for an overlap ratio d_{OL}, can be obtained using (11), provided $0 \leq d_{OL} \leq min(d_1, d_2)$.

$$\begin{aligned} \theta_L &= (d_1 - d_{OL})T = \quad t_2; \text{ for right shift of } S_2 \\ \theta_R &= -(d_2 - d_{OL})T = -t_1; \text{ for left shift of } S_2 \end{aligned} \tag{11}$$

Multiple control parameters of TSBC, namely d_1, d_2 and d_{OL}, provide higher DoFoC in comparison to CBC in which d_2 is the only controllable parameter. The presence of the additional S_1-D_1 pair also help improve the voltage gain.

IV. IMPROVEMENT IN VOLTAGE GAIN

To demonstrate the improvement in voltage gain, the proposed TSBC is compared with CBC. In (6), the voltage relation of TSBC is presented as a function of the switching intervals. However, a relation in terms of duty ratios provides a more perceptive representation for the purpose of comparison. Substituting time intervals from (10) in the voltage relation of (6), the voltage gain of TSBC is obtained as

$$G_v = \frac{1 - d_1}{1 - d_1 - d_2} \quad ; \quad d_1 + d_2 < 1 \tag{12}$$

The CBC has only one switch and operates in two states which correspond to states 0 and 2 of TSBC. Hence, if S_1 is turned off throughout the operation of the converter, the proposed TSBC performs identical to CBC. The time intervals in CBC is obtained as $t_1 = t_3 = 0$ and $t_0 + t_2 = T$, and duty ratio $d_1 = 0$. The voltage gain of CBC is as in (13).

$$G_{vC} = \quad \frac{T}{t_0}; \ (t_0 > 0) \quad = \frac{1}{1 - d_2}; \ (d_2 < 1) \tag{13}$$

The voltage gain ratios of CBC and TSBC, G_{vC} and G_v, for varying duty ratios are presented in Fig. 4. The duty ratio d_2 is varied continuously while d_1 takes values from 0 to 0.8. Considering the constraint of $d_1 + d_2 < 1$ from (12), the operating and non-operating ranges of TSBC are indicated in Fig. 4. When d_1=0, the voltage gain of the TSBC is identical to that of the CBC. On the other hand, if $d_1 > 0$, the TSBC is capable of operating at higher voltage gains. For instance, at d_2=0.7, the voltage gain of CBC (d_1=0) is 3.33. If d_1 is varied to 0.1 and 0.2 while d_2 remains at 0.8, the voltage gain of TSBC is increased to 4.5 (35% increase) and 8 (140% increase) respectively. This improved voltage gain effectively implies that the operating range of TSBC is improved.

From (12), the voltage gain ratio G_v is noticed to be independent of the overlap ratio d_{OL}. As a result, the phase shift on the switching pulse S_2 w.r.t. S_1 has no effect on the voltage gain. The same voltage gain can be obtained with multiple choices of duty ratios, thereby increasing the DoFoC which is further explained in the following section.

V. INCREASE IN DoFoC AND CHOICE OF DUTY RATIOS

In CBC, the magnitude and ripples of the currents and voltages vary with the gain ratio and cannot be controlled as it has only one control variable d_1 i.e. one DoFoC. However, the proposed TSBC has more than one combination of d_1, d_2 and d_{OL} that yield the same voltage gain, which implies multiple DoFoC. Duty ratios can be chosen in accordance with multiple constraints in addition to voltage gain such as magnitude and ripple of currents and voltages, switching frequency, and/or switching losses. In this paper, the output ripple voltage ΔV_o and inductor current ripple ΔI_L are considered for the choice of duty ratios. Similar analysis can be performed for other parameters, such as inductor current magnitude, based on the application. The voltage gain G_v and switching frequency $f_{sw} = \frac{1}{T}$ are predefined. Additionally, for the simplicity of analysis and implementation, complete overlap case is assumed here. Therefore, the overlap ratio between the two switching pulse is fixed based on the following conditions.

$$\begin{aligned} d_{OL} &= d_1 \quad , \qquad \text{If } d_1 < d_2 \\ d_{OL} &= d_2 \quad , \qquad \text{If } d_1 > d_2 \\ \therefore d_{OL} &= min(d_1, d_2) \end{aligned} \tag{14}$$

A. CASE 1: INDUCTOR CURRENT MAGNITUDE

The inductor is often a sizable component in converters. Therefore, limiting the inductor current to an optimal value is considered appropriate to reduce the weight, size and cost of converter. Further, a control on the inductor current is useful to control input/output currents based on the application. If the inductor current is limited by the equation $I_L = xI_o$, the following relation is obtained from (9).

$$x = \frac{I_L}{I_o} = \frac{1}{(1 - d_1 - d_2)} \tag{15}$$

From (15), it can be observed that the inductor current ratio is independent of the overlap ratio d_{OL}. Solving (15) using (19),

we obtain the values of d_1 and d_2 as shown in(16).

$$[d_1, d_2] = \left[1 - \frac{G_v}{x}, \frac{G_v - 1}{x}\right] \tag{16}$$

Since the duty ratios are expected to be non-negative, the above equation results in the constraint $x \geq G_v$. Based on the duty ratios obtained from (16), switching pulses can be generated to attain the desired voltage gain G_v and inductor current ratio x, and thereby control both output voltage V_o and inductor current I_L.

B. CASE 2: OUTPUT VOLTAGE RIPPLE RATIO

Many applications involve loads that require the output voltage V_o to be stable with minimal ripple ΔV_o. Using circuit analysis, the ripple voltage can be expressed as in (17).

$$\Delta V_o = \frac{V_o}{R_o C_o f_{sw}} \frac{(1 - d_1 - d_2 + d_{OL})(d_1 + d_2)}{(1 - d_1 - d_2)} \tag{17}$$

Let the output voltage ripple ratio be $\Delta y = \frac{\Delta V_o}{V_o}$. Considering this limit on ripple voltage, we obtain the following relation.

$$\Delta y = \frac{1}{R_o C_o f_{sw}} \frac{(1 - d_1 - d_2 + d_{OL})(d_1 + d_2)}{(1 - d_1 - d_2)} \tag{18}$$

From voltage gain of (12), the duty ratio d_1 is expressed as

$$d_1 = 1 - \frac{d_2 G_v}{G_v - 1} \tag{19}$$

Substituting d_{OL} and d_1 from (14) and (19) in (18), the following relation is obtained for output voltage ripple ratio.

$$\Delta y = \frac{1}{R_o C_o f_{sw}} \begin{cases} (1 - d_2)\left(\frac{G_v - 1}{d_2} - 1\right); \text{if } d_1 < d_2 \\ G_v\left(1 - \frac{d_2}{G_v - 1}\right); \text{if } d_1 > d_2 \end{cases} \tag{20}$$

The duty ratio d_2 is obtained by solving (20) and d_1 is obtained by substituting this value of d_2 to (19). The values of duty ratios and overlap ratio thus obtained will result in the specified gain G_v and ripple ratio Δy of the output voltage.

C. CASE 3: INDUCTOR CURRENT RIPPLE RATIO

The inductor current ripple is one of the factors that define the inductor value for CCM operation. Hence, operating the converter at a predefined inductor current ripple can ensure CCM operation. The ripple current ΔI_L is correlated to the inductor L as per (21), where Δt is the interval during which I_L changes by ΔI_L and v_L is the voltage across it during Δt.

$$v_L = L \frac{\Delta I_L}{\Delta t} \tag{21}$$

Substituting ΔI_L and v_L during the switching state t_0 from Table 1 and using the voltage gain in (12), the inductor current ripple ΔI_L can be expressed as (22).

$$\Delta I_L = \frac{V_o}{L f_{sw}} \frac{(1 - d_1 - d_2 + d_{OL}) d_2}{(1 - d_1)} \tag{22}$$

From the current relations in (9), the inductor current can be defined in terms of duty ratios by (23).

$$I_L = \frac{V_o}{R_o} \frac{T}{(t_0 - t_3)} = \frac{V_o}{R_o} \frac{1}{(1 - d_1 - d_2)} \tag{23}$$

If the ripple current ratio is fixed to Δx, i.e. $\Delta I_L = \Delta x \times I_L$,

$$\Delta x = \frac{R_o}{L f_{sw}} \frac{(1 - d_1 - d_2 + d_{OL}) d_2}{G_v} \tag{24}$$

Substituting d_{OL} and d_1 from (14) and (19),

$$\Delta x = \frac{R_o}{L f_{sw}} \begin{cases} \frac{(1 - d_2) d_2}{G_v}; \text{if } d_1 < d_2 \\ \frac{d_2^2}{G_v - 1}; \text{if } d_1 > d_2 \end{cases} \tag{25}$$

Solving (25), (19) and (14) in order yields the values of d_2, d_1 and d_{OL} respectively that results in the specified inductor current ripple ratio Δx while retaining the voltage gain at G_v.

VI. OPTIMAL SELECTION OF COMPONENTS

The size and cost of a converter are determined by the ratings of its constituent components. The design of components used in TSBC is detailed as follows. The sizing of switches, diodes, inductor, and capacitors are based on rated values of parameters such as input voltage V_{in}, switching frequency f_{sw}, rated output voltage V_{oR}, and rated power $S_R = V_{oR} I_{oR}$. These parameters are assumed to be fixed prior to design.

A. INDUCTOR

The rating of the inductor is decided based on the maximum of average and ripple currents through it. The ripple current decides the inductor value while the average current determines the current rating of the inductor. The maximum ripple current $\Delta I_{L_{max}}$ is required to be limited to Δx=(10 to 30)% of the rated inductor current I_{LR}. Since the inductor current and output current can be related by (9), the maximum ripple current at rated condition is expressed in terms of V_{oR} as (26).

$$\Delta I_{L-max} = \Delta x_{max} I_{LR} = \frac{\Delta x S_R}{(1 - d_1 - d_2) V_{oR}} \tag{26}$$

During all operating conditions, the inductor current is expected to satisfy the condition $\Delta I_L < \Delta I_{L-max}$. Therefore, from (22) and (26), the limit for inductance L is obtained as

$$L \geq \frac{V_{oR} V_{in}}{\Delta x S_R f_{sw}} (d_2(1 - d_1 - d_2 + d_{OL}))_{max} \tag{27}$$

Considering d_{OL} from (14), $(d_2(1 - d_1 - d_2 + d_{OL}))_{max}$=0.25. Therefore, the minimum value of inductor is

$$L_{min} = \frac{0.25 V_{oR} V_{in}}{\Delta x S_R f_{sw}} \tag{28}$$

In addition to the inductor value, the component specification of inductor includes the average current through it at rated operating conditions of the converter. The rated inductor current I_{LR} can be derived from (9) as

$$I_{LR} = \frac{S_R}{V_{oR}(1 - d_1 - d_2)_{max}} \tag{29}$$

The sum of duty ratios $d_1 + d_2$ is limited to 0.9 to enable efficient operation of the converter. Therefore, the maximum inductor current can be expressed as in

$$I_{L-max} = \frac{10 S_R}{V_{oR}} \tag{30}$$

The minimum inductor value from (28) and its current rating from (30) are used for the choice of a suitable inductor.

TABLE 2. Voltages and currents of the switching components.

Specification		State 0	State 1	State 2	State 3
Diode D_1	V_{D_1}	0	0	$V_{in} - V_o$	$V_{in} - V_o$
	I_{D_1}	I_L	I_L	0	0
Switch S_1	V_{S_1}	$V_o - V_{in}$	$V_o - V_{in}$	0	0
	I_{S_1}	0	0	I_L	I_L
Diode D_2	V_{D_2}	0	$-V_o$	0	$-V_o$
	I_{D_2}	I_L	0	I_L	0
Switch S_2	V_{S_2}	V_o	0	V_o	0
	I_{S_2}	0	I_L	0	I_L

B. CAPACITORS

The capacitors in a converter are chosen based on the ripple and maximum values of voltages. The ripple voltage ΔV_C across a capacitor C can be related to its capacitance by (31).

$$i_C = C\frac{\Delta V_C}{\Delta t} \tag{31}$$

Hence, from Table 1, the ripples of input and output voltages of the proposed TSBC are obtained as (32) and (33).

$$\Delta V_{in} = \frac{(t_2+t_3)I_{in}}{C_{in}} = \frac{d_1 G_v S_R}{C_{in} f_{sw} V_{oR}} \tag{32}$$

$$\Delta V_o = \frac{t_0(I_L - I_o)}{C_o} = \frac{(1-d_1-d_2+d_{OL})(d_1+d_2)S_R}{(1-d_1-d_2)C_o f_{sw} V_{oR}} \tag{33}$$

The maximum ripple ΔV_C is often limited as $\Delta y = (5 \text{ to } 10)\%$ of the rated capacitor voltage V_C. If Δy_{in} and Δy are the limits of ripples in ΔV_{in} and ΔV_o respectively, i.e. $\Delta V_{in-max} = \Delta y_{in} V_{in}$ and $\Delta V_{o-max} = \Delta y V_o$ the constraint on capacitor ratings can be calculated using (34) and (35).

$$C_{in} \geq \frac{S_R}{\Delta y_{in} V_{oR} V_{in} f_{sw}} (d_1 G_v)_{max} \tag{34}$$

$$C_o \geq \frac{S_R}{\Delta y V_{oR}^2 f_{sw}} \left((d_1+d_2)\left(1+\frac{d_{OL}}{1-d_1-d_2}\right)\right)_{max} \tag{35}$$

Assuming the range of duty ratios is limited by $d_1 + d_2 \leq 0.9$ to avoid low efficiency operation, the values of $(d_1 G_v)_{max}$ and $\left((d_1+d_2)\left(1+\frac{d_{OL}}{1-d_1-d_2}\right)\right)_{max}$ are obtained as 2.5 and 4.95 respectively. Substituting these in (34) and (35), the minimum value of capacitors are obtained as

$$C_{in\text{-}min} = \frac{2.5 S_R}{\Delta y_{in} V_{oR} V_{in} f_{sw}} \tag{36}$$

$$C_{o\text{-}min} = \frac{4.95 S_R}{\Delta y V_{oR}^2 f_{sw}} \tag{37}$$

The maximum voltages across the capacitors C_{in} and C_o are V_{in} and V_{oR} respectively. These voltage ratings and the corresponding capacitor values from (34) and (35) are used for the selection of capacitors.

C. SWITCHES AND DIODES

The specification of switches and diodes are decided based on the maximum voltage, current and switching frequency. Assuming loss-less components, the voltages and currents through the switching components are determined by circuit analysis for four states of operation and listed in Table 2.

TABLE 3. Comparison of component specification of TSBC and CBC.

Components			CBC	TSBC
Existing in CBC	L	L_{min}	$\frac{d_2(1-d_2)V_{oR}V_{in}}{\Delta x S_R f_{sw}}$	$\frac{d_2(1-d_1-d_2+d_{OL})V_{oR}V_{in}}{\Delta x S_R f_{sw}}$
		I_{max}	$\frac{S_R}{(1-d_2)V_{oR}}$	$\frac{S_R G_v}{(1-d_1-d_2)V_{oR}}$
	C_o	C_{min}	$\frac{d_2 S_R}{\Delta y V_{oR}^2 f_{sw}}$	$\frac{(d_1+d_2)(1-d_1-d_2+d_{OL})S_R}{(1-d_1-d_2)\Delta y V_{oR}^2 f_{sw}}$
		V_{max}	V_{oR}	V_{oR}
	S_2, D_2	V_{max}	V_{oR}	V_{oR}
		I_{max}	$\frac{S_R G_v}{(1-d_2)V_{oR}}$	$\frac{S_R G_v}{(1-d_1-d_2)V_{oR}}$
Cascaded	S_1, D_1	V_{max}	-	$V_{oR} - V_{in}$
		I_{max}	-	$\frac{S_R G_v}{(1-d_1-d_2)V_{oR}}$

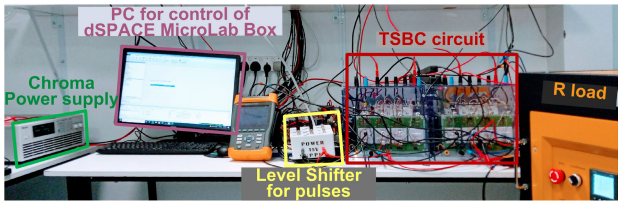

FIGURE 5. Hardware setup for experimental validation of proposed TSBC.

The current ratings of the switching devices in TSBC can be calculated as (38).

$$I_{S_1max} = I_{S_2max} = I_{D_1max} = I_{D_2max} = \frac{10 S_R}{V_{oR}} \tag{38}$$

Similarly, the voltage rating of switch-diode pairs (S_1,D_1) and (S_2,D_2) are obtained as (39) and (40) respectively.

$$V_{S_1max} = V_{D_1max} = V_{oR} - V_{in} \tag{39}$$

$$V_{S_2max} = V_{D_2max} = V_{oR} \tag{40}$$

The switching components of the proposed TSBC are thereby determined using (38), (39) and (40).

D. COMPARISON OF SPECIFICATIONS WITH CBC

In an existing CBC based system, the voltage gain and DoFoC can be improved by implementing TSBC by cascading the CBC with an extra switch-diode pair. For this to be practically feasible, the component specifications of the proposed TSBC should be comparable to CBC. Hence, a comparison of the component ratings in both converters is presented in Table 3 and discussed further to validate the viability of incorporating TSBC into the conversion system with an existing CBC.

The ratings of components in CBC are considered to be a function of d_2 while those of TSBC depend on d_1, d_2 and d_{OL}. To avoid low efficiency operation of CBC, d_2 is often limited, to say 0.9. Similarly, in TSBC, the sum of duty ratios d_1+d_2 is limited to 0.9 while d_{OL} is set to $min(d_1, d_2)$. Considering these limits, the specifications of the components in Table 3 for CBC and TSBC are found to be identical. The additional components in TSBC, S_1 and D_1, have the same current ratings and reduced voltage ratings as the

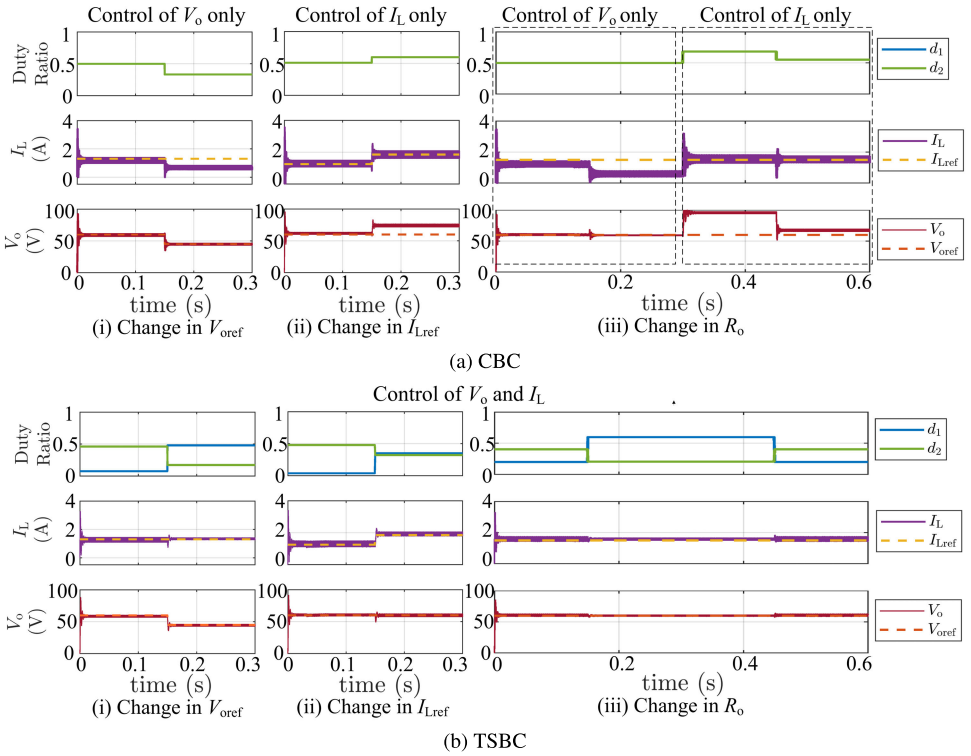

FIGURE 6. Simulation results to show improvement in DoFoC of the proposed TSBC in comparison to CBC.

TABLE 4. Ratings used in simulation and hardware prototype.

Parameter	Value
Rated Power P_R	170 W
Input voltage V_{in}	30 V
Rated output voltage V_{oR}	180 V
Switching frequency f_{sw}	10 kHz
Inductance L	4 mH
Input Capacitance C_{in}	50 μF
Output Capacitance C_o	7.5 μF

TABLE 5. Output voltage and inductor current as functions of duty ratios.

Converter	V_o	I_L
CBC	$V_{in}\frac{1}{(1-d_2)}$	$\frac{V_{in}}{R_o}\frac{1}{(1-d_2)^2}$
TSBC	$V_{in}\frac{1-d_1}{(1-d_1-d_2)}$	$\frac{V_{in}}{R_o}\frac{1-d_1}{(1-d_1-d_2)^2}$

other switching components. The comparable ratings of all constituent components support TSBC implementation by cascading a switch-diode pair with an existing CBC.

VII. RESULTS AND DISCUSSION

The theoretical analysis of the proposed TSBC is verified using simulations on MATLAB/Simulink platform and hardware prototype shown in Fig. 5. A constant input voltage of 30 V and resistive load 170 W are considered. The ratings of the converter are specified in Table 4. The performance of the TSBC is assessed using an open-loop control implemented using dSPACE MicroLab Box with duty ratios values considering $d_1 + d_2 < 0.85$ and $d_{OL} = min(d_1,d_2)$. The results of TSBC with $d_1 = 0$ are regarded similar to those of CBC.

A. VALIDATING IMPROVED DoFoC

To highlight the effect of improved DoFoC of the proposed TSBC, open-loop controls are implemented and the duty ratios are calculated for predefined variables such as V_{in}, V_o, R_o and I_L. The results of TSBC are compared with those of CBC to highlight the improvement in DoFoC.

From (12), (13) and (16), the output voltage and inductor current in CBC and TSBC can be expressed in terms of duty ratios as shown in Table 5. Here, the input voltage V_{in} and output resistance R_o are considered known variables. Based on the equations for CBC in Table 5, if an output voltage of $V_o = 60\ V$ is to be obtained from an input voltage $V_{in} = 30\ V$, only one value of duty ratio, i.e. $d_2 = 0.5$, can be used. The inductor current in CBC is as function of this duty ratio and thus cannot be independently controlled. Similarly, if I_L is controlled using d_2, V_o cannot be controlled to any required value as it is dependent on and only on d_2. Note that here the input voltage V_{in} and output resistance R_o are not used for control. On the contrary to CBC, there exists multiple combinations of $[d_1, d_2]$ for TSBC, that can be used to obtain an output voltage of $V_o = 60\ V$ from $V_{in} = 30\ V$. This is because when only V_o is controlled, it results in only one

TABLE 6. Comparison of control of V_o and I_L in CBC and TSBC.

Converter	Fig.	Control	Time (s)	V_{oref} (V)	I_{Lref} (A)	R_o (Ω)	d_1	d_2	V_o (V)	I_L (A)
CBC	6(a)(i)	V_o	$0 < t < 0.15$ $0.15 < t < 0.30$	60 45	-	100	-	0.5 0.33	60 45	1.28 0.79
TSBC	6(b)(i)	V_o, I_L	$0 < t < 0.15$ $0.15 < t < 0.30$	60 45	1.3	100	0.08 0.48	0.46 0.173	60 45	1.3
CBC	6(a)(ii)	I_L	$0 < t < 0.15$ $0.15 < t < 0.30$	-	1.25 1.85	100	-	0.51 0.59	60 74	1.24 1.85
TSBC	6(b)(ii)	V_o, I_L	$0 < t < 0.15$ $0.15 < t < 0.30$	60	1.25 1.85	100	0.04 0.35	0.48 0.32	60	1.25 1.86
CBC	6(a)(iii)	V_o	$0 < t < 0.15$ $0.15 < t < 0.30$	60	-	100 200	-	0.5	60	1.28 0.62
		I_L	$0.30 < t < 0.45$ $0.45 < t < 0.60$	-	1.5	200 100	-	0.68 0.55	96 68	1.51
TSBC	6(b)(iii)	V_o, I_L	$0 < t < 0.15$ $0.15 < t < 0.30$ $0.30 < t < 0.45$ $0.45 < t < 0.60$	60	1.5	100 200 100	0.20 0.59 0.20	0.40 0.20 0.40	60 60 60	1.52 1.53 1.52

equation with two variables $[d_1, d_2]$, thereby yielding multiple solutions. To obtain unique solutions for $[d_1, d_2]$, another non-redundant equation can be considered. This implies that an additional variable can be controlled and thereby indicates increased DoFoC. In this example, in addition to V_o, the inductor current I_L is considered to solve for $[d_1, d_2]$. The results are presented in Fig 6a and the specific values are mentioned in Table 6 for the purpose of comparison.

It is noticed from Fig. 6, for CBC, one variable, i.e. either V_o or I_L can be controlled using d_2. On the other hand, from Fig. 6b for TSBC, it is observed that both V_o and I_L can be controlled simultaneously using d_1 and d_2. This validates the increased DoFoC due to the switch-diode pair in TSBC.

B. CONTROL OF RIPPLE RATIOS USING DoFoC

The increased DoFoC is further validated by operating the TSBC at different voltage gain ratios while retaining constant ripple ratios as shown in Fig. 7a. The duty ratios are chosen based on (20) and (25) for constant output voltage ripple ratio and inductor current ripple ratio respectively. For simplicity of switching pulse generation, the overlap ratio between the two switching pulse is fixed as $min(d_1, d_2)$.

In Fig. 7a, the results for constant output voltage ripple ratio of $\Delta y = 0.06$ are presented. The duty ratios calculated based on (20) are $[d_1, d_2]$=[(0.275, 0.242), (0.15, 0.425), (0.09, 0.54), (0.01, 0.743)] for voltage gains of G_v = [4, 1.5, 2.25]. Output voltages of V_o=[43.56, 58.43, 72.42, 116.5] V and practical voltage gains of [1.45, 1.94, 2.41, 3.88] are achieved with these duty ratios. The inductor current and output voltage ripple increases with the voltage gain. Nevertheless, the output voltage ripple ratio $\Delta y = \frac{\Delta V_o}{V_o}$ remains approximately constant at 0.06, thereby validating the calculation based on (20).

Fig. 7b presents the results for a constant inductor current ripple ratio of $\Delta x = 0.3$. For the voltage gains G_v = [4, 1.5, 2, 2.5] the duty ratios are calculated based on (25) as $[d_1, d_2]$=[(0.5, 0.167), (0.52, 0.24), (0.52, 0.288), (0.11, 0.667)]. From the results, the output voltage is observed to increase from 43.56 V to 58 V, 71.54 V and 115.4 V as the duty ratios are varied, thereby yielding practical voltage gains of 1.45, 1.93, 2.38 and 3.85. The magnitude and ripple of inductor current, I_L and ΔI_L increase with the gain, while the ripple ratio $\Delta x = \frac{\Delta I_L}{I_L}$ remains at approximately at the expected value of 0.3, thus validating (25) and related theoretical analysis.

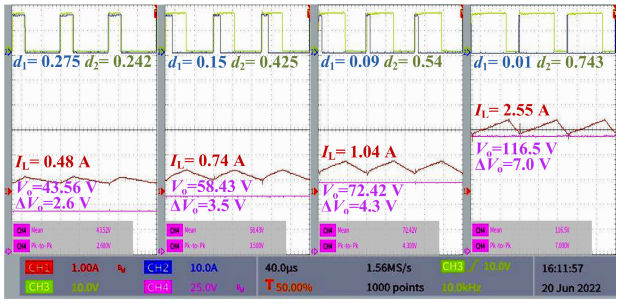

(a) Experimental results for constant Δy=0.06

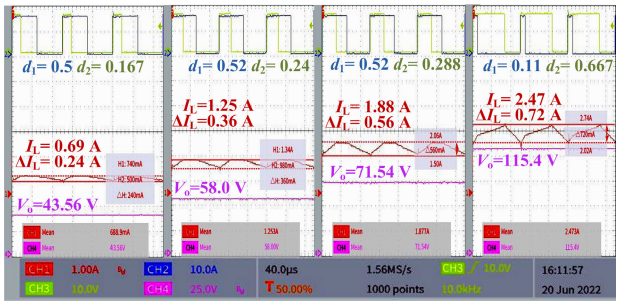

(b) Experimental results for constant Δx=0.3

FIGURE 7. Experimental results for different voltage gains and constant ripple ratios to validate increased DoFoC.

C. IMPROVED VOLTAGE GAIN DUE TO S_1-D_1 PAIR

In addition to the increase in DoFoC, the additional switch-diode pair (S_1-D_1) in TSBC provides improved volt-

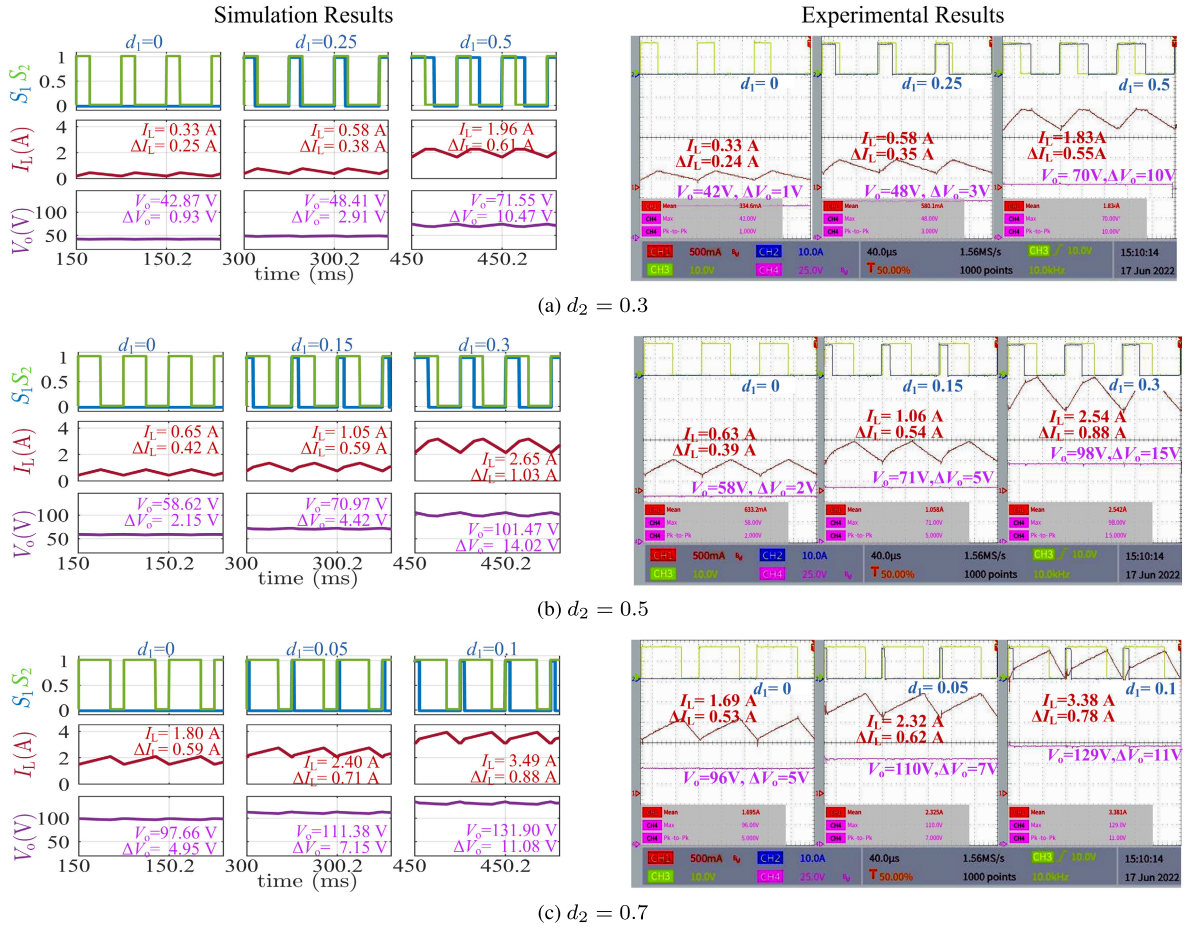

FIGURE 8. Simulation and experimental results showing effect of change in d_1 on the voltage gain G_V.

age gain in comparison to CBC. The effect of S_1-D_1 pair on the voltage gain ratio is observed by varying d_1 for constant values of d_2 = [0.3, 0.5, 0.7]. The resulting waveforms in simulation and experiment are presented in Fig. 8. The results with $d_1 = 0$ are identical to those of CBC.

The results for d_1=(0, 0.25, 0.5) and d_2=0.3 is shown in Fig. 8a. These duty ratios yield, in simulation, average output voltages V_o = (42.87, 48.41, 71.55) V with voltage ripples ΔV_o = (0.86, 2.46, 7.24) V and inductor current I_L = (0.33, 0.58,1.96) A with ΔI_L = (0.25, 0.38, 0.61) A. For the same case, the average and ripple values obtained using the experiment prototype are $[V_o, \Delta V_o]$ = [(42, 48, 70), (1, 3, 10)] V and $[I_L, \Delta I_L]$=[(0.33, 0.58, 1.83), (0.24, 0.35, 0.55)] A. From these values, the output voltage is noticed to increase with d_1 while d_2 remains constant at 0.3, indicating increase in voltage gain.

Similarly, Fig. 8b presents the results for d_1 = (0, 0.25, 0.5) and d_2 = 0.5. In simulation, these duty ratios yield average output voltages of V_o = (58.62, 70.97, 101.47) V with ΔV_o = (2.15, 4.42, 14.02) V and inductor current of I_L = (0.65, 1.05,2.65) A with ΔI_L = (0.42, 0.59, 1.03) A. The average and ripple values obtained for the same case using the experimental prototype are $[V_o, \Delta V_o]$ = [(58,71,98), (2,5,15)] V and $[I_L, \Delta I_L]$ = [(0.63,1.06,2.54), (0.39, 0.54, 0.88)] A. From these values, V_o is noticed to increase with d_1 while d_2 remains constant at 0.5. Similar observations can be made from the results of d_2 = 0.7 in Fig. 8c. This validates the improvement of voltage gain using the control of d_1.

TABLE 7. Effect of change in d_1 on G_V, Δx and Δy.

d_2	d_1	G_v			Δx			Δy		
		Calc.	Sim.	Exp.	Calc.	Sim.	Exp.	Calc.	Sim.	Exp.
0.5	0	2	1.95	1.93	0.59	0.60	0.61	0.035	0.036	0.034
	0.15	2.43	2.37	2.37	0.49	0.49	0.5	0.065	0.062	0.070
	0.3	3.5	3.38	3.27	0.34	0.34	0.34	0.014	0.014	0.015
0.7	0	3.33	3.25	3.2	0.29	0.30	0.31	0.049	0.051	0.052
	0.05	3.8	3.71	3.67	0.26	0.26	0.27	0.063	0.064	0.064
	0.1	4.5	4.39	4.3	0.22	0.22	0.23	0.084	0.084	0.085

The voltage gain G_v, output voltage ripple ratio Δy, inductor current ripple ratio Δx obtained by theoretical calculation (Calc.), simulation (Sim.) and experiment (Exp.) are summarized in Table 7 for the ease of comparison. For all the duty ratios considered, the calculated voltage gain and ripple

TABLE 8. Comparison of TSBC with existing improved DC–DC converter topologies.

Converter Topology	Voltage Gain	Component Count				System Rating				Efficiency	Claims
		S	D	C	L	V_{in} (V)	V_o (V)	P (W)	f_{sw} (kHz)	η (%)	
Soft-switching cascade boost converter [26]	$\frac{1}{(1-d)^2}$	2	5	4	3	30-50	300	300	50	93.4	High-gain; wider turn-off time
Quadratic boost converter [27]	$\frac{1}{(1-d)^2}$	1	3	2	2	50	200	67	70	96.2	Low buffer capacitor voltage stress
Dual-boost DC-DC converter [28]	$\frac{1}{(1-d)^2}$	1	3	2	2	48	150	100	20	94.0	High gain & efficiency; Low switch stress
Cascaded single-switch DC-DC converter [29]	$\frac{k(n+1)+n(d-1)}{(1-d)^2}$	1	4	3	2	20	400	280	40	93.3	High step-up; Low switch stress
Cascaded boost converter [30]	$\frac{1}{(1-d)^2}$	1	3	2	2	24	(Sim)350 (Exp)100	(Sim)300 (Exp) 60	20	92.0	High boost with single switch
Cascaded synchronous converter with ZVS [31]	$\frac{1+nd}{(1-d)^2}$	2	3	2	3	24	200	200	50	93.0	High gain; Improved efficiency
Soft-switching DC-DC converter [18]	$\frac{1}{1-d}$	3	1	1	2	48	100	500	100	97.6	Soft-switching; 2DoFoC
Proposed TSBC	$\frac{1-d_1}{1-d_1-d_2}$	2	2	1	1	30	180	170	10	96.2	Improve gain & DoFoC with S-D leg cascaded to CBC

d, d_1, d_2=duty ratio, n=coupled inductor turns ratio, k=coupling coefficient — S- Switch, D- Diodes, C- Capactiors, L- Inductors

ratios are observed to be comparable with those obtained in simulation and experiment. This validates the theoretical analysis presented in the paper. For a constant value of d_2, say 0.3, the calculated voltage gain G_v increases from 1.43 to 1.67 and 2.5 with d_1= 0, 0.25 and 0.5 respectively. Both simulation and experimental results for voltage gain are consistent with these theoretical values. The inductor ripple current ratio is observed to reduce as d_1 increases. Therefore, TSBC can restrain the inductor current ripple ratio at higher voltage gains due to the additional switch-diode pair. Although the output ripple voltage rises with d_1, it can be limited by utilizing the additional DoFoC feature of the proposed converter which is detailed further in the subsequent discussion of results. If Δy_{in} and Δy are the limits of ripples in ΔV_{in} and ΔV_o respectively, i.e. $\Delta V_{in-max} = \Delta y_{in} V_{in}$ and $\Delta V_{o-max} = \Delta y V_o$ the constraint on capacitor ratings can be calculated using (34) and (35).

The above results indicate that the addition of a switch-diode leg at the CBC can aid to improve the voltage gain ratio as well as the DoFoC. Hence, the proposed TSBC can be used to control other circuit parameters, such as inductor current or voltage/current ripple ratios in addition to the evident control on voltage gain.

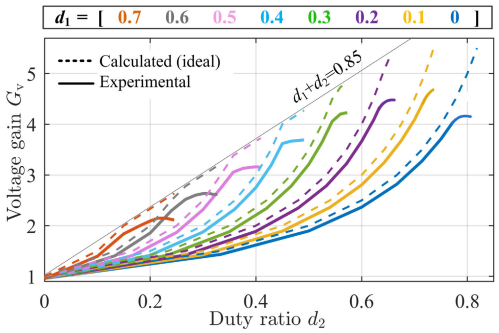

(a) Comparison of theoretical and experimental gain

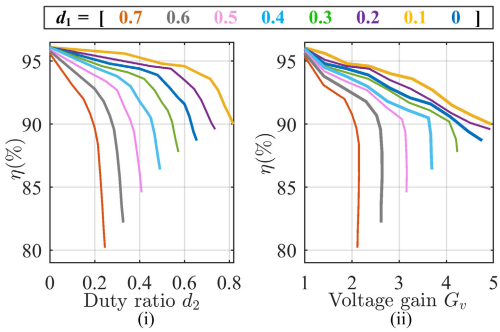

(b) Experimental efficiency for varying d_2 and G_v

FIGURE 9. Experimental gain and efficiency for different d_1 values.

D. ANALYSIS OF EXPERIMENTAL EFFICIENCY

The experimental voltage gain and efficiency of the proposed TSBC for different duty ratio values are presented in Fig. 9a for the rated operating condition. In Fig. 9, the theoretically calculated gain is validated using the experimentally obtained voltage gain values. The duty ratios d_1 and d_2 are limited by the inequalities $d_1 < 0.85$, $d_2 < 0.85$ and $d_1 + d_2 < 0.85$ to avoid converter operation at very low efficiency. It is noted that the calculated and experimental gain values are comparable for most values of d_1 and d_2. However, as the sum $d_1 + d_2$ approaches 0.85, the experimental values of voltage gain varies from the calculated ideal values. This is owing to losses incurred in the switches at high duty ratios and output voltages as can be observed from the efficiency plots in Fig. 9b. Fig. 9(i) and (ii) illustrate the relation of experimental efficiency η with d_2 and G_v respectively. The maximum efficiency is observed as 96.2% and competent efficiency is observed for the range $d_1 + d_2 < 0.7$. The experimental efficiency reduces with increase in d_2 and G_v.

The proposed TSBC can be considered as a derived topology of the CBC by cascading a switch-diode pair to bring about an improvement in voltage gain and DoFoC. There exist several derived or cascaded topologies that achieve improved variations its substituent converters. Among these, the relevant converter topologies are compared with TSBC to highlight its many advantages. Table 8 compares the experimental efficiency of the proposed TSBC is compared with other cascaded converter configurations alongside other parameters such as voltage gain and component count. Since the experimental efficiency are obtained at different system ratings for different converters in the existing literature, the voltage, power and frequency rating at which the converter topology was tested is also listed in Table 8. In comparison, the proposed TSBC has the least number of passive components as well as the least overall component count. This contributes to reduced size and initial cost of the converter. Additionally, the efficiency of TSBC is on par with that of existing converters, including those that use soft switching. The proposed converter is also observed to be the most comparable topology to CBC and hence can easily replace CBC in existing systems without inclusion of additional passive components or complex changes in circuit and control. Hence, the range of application for the proposed TSBC can be considered as all power conversion systems that conventionally employ CBC, for example, within the power conversion interface of a PV-based stand-alone or grid connected system.

VIII. CONCLUSION

In this paper, a two-switch boost converter is proposed to enhance the voltage gain and increase the DoFoC in power conversion interfaces. The circuit of TSBC is analysed for its four states of operation based on which the voltage and current ratios are derived. The combination of switching pulses for different duty ratios and overlap ratio is detailed and the improvement in voltage gain ratio is presented with a comparison to CBC. The formulations related to the choice of duty ratios based on the ripple ratios of output voltage and inductor current are derived to demonstrate the improved DoFoC of TSBC. The design of constituent components in TSBC are discussed. The simulation and experimental results validate the theoretical claims of TSBC presented in this paper. The experimental results indicate that for a duty ratio of 0.7 for the existing switch of CBC, an increase in voltage gain from 3.2 to 4.3 is achieved when the duty ratio of the additional switch in TSBC is varied from 0 to 0.1. Similarly, improved DoFoC is demonstrated with inductor current control as well as with constant ripple ratios while maintaining the required output voltage. The proposed converter can easily replace the commonly CBC to improve the gain and DoFoC by introducing only two additional components at the input side of the circuit.

REFERENCES

[1] H. Zhang, D. Dong, M. Jing, W. Liu, and F. Zheng, "Topology derivation of multiple-port DC–DC converters based on voltage-type ports," *IEEE Trans. Ind. Electron.*, vol. 69, no. 5, pp. 4742–4753, May 2022.

[2] H. Ardi, A. Ajami, and M. Sabahi, "A novel high step-up DC–DC converter with continuous input current integrating coupled inductor for renewable energy applications," *IEEE Trans. Ind. Electron.*, vol. 65, no. 2, pp. 1306–1315, Feb. 2018.

[3] M. S. Bhaskar, V. K. Ramachandaramurthy, S. Padmanaban, F. Blaabjerg, D. M. Ionel, M. Mitolo, and D. Almakhles, "Survey of DC-DC non-isolated topologies for unidirectional power flow in fuel cell vehicles," *IEEE Access*, vol. 8, pp. 178130–178166, 2020.

[4] M. L. Alghaythi, R. M. O'Connell, N. E. Islam, M. M. S. Khan, and J. M. Guerrero, "A high step-up interleaved DC-DC converter with voltage multiplier and coupled inductors for renewable energy systems," *IEEE Access*, vol. 8, pp. 123165–123174, 2020.

[5] M. Meraj, M. S. Bhaskar, B. P. Reddy, and A. Iqbal, "Non-isolated DC–DC power converter with high gain and inverting capability," *IEEE Access*, vol. 9, pp. 62084–62092, 2021.

[6] W. Li and X. He, "Review of nonisolated high-step-up DC/DC converters in photovoltaic grid-connected applications," *IEEE Trans. Ind. Electron.*, vol. 58, no. 4, pp. 1239–1250, Apr. 2011.

[7] A. Amir, A. Amir, H. S. Che, A. Elkhateb, and N. A. Rahim, "Comparative analysis of high voltage gain DC-DC converter topologies for photovoltaic systems," *Renew. Energy*, vol. 136, pp. 1147–1163, Jun. 2019.

[8] Y. Koç, Y. Birbir, and H. Bodur, "Non-isolated high step-up DC/DC converters—An overview," *Alexandria Eng. J.*, vol. 61, no. 2, pp. 1091–1132, 2022.

[9] G. G. Ramanathan and N. Urasaki, "Non-isolated interleaved hybrid boost converter for renewable energy applications," *Energies*, vol. 15, no. 2, p. 610, Jan. 2022.

[10] J. Supriya and J. S. Rajashekar, "A comprehensive review of various isolated DC-DC converters topologies associated with photovoltaic applications," *Recent Adv. Electr. Electron. Eng., Formerly Recent Patents Electr. Electron. Eng.*, vol. 15, no. 8, pp. 595–606, Dec. 2022.

[11] T. Pereira, F. Hoffmann, R. Zhu, and M. Liserre, "A comprehensive assessment of multiwinding transformer-based DC–DC converters," *IEEE Trans. Power Electron.*, vol. 36, no. 9, pp. 10020–10036, Sep. 2021.

[12] V. K. Goyal and A. Shukla, "Isolated DC–DC boost converter for wide input voltage range and wide load range applications," *IEEE Trans. Ind. Electron.*, vol. 68, no. 10, pp. 9527–9539, Oct. 2021.

[13] J. Ahmad, M. Zaid, A. Sarwar, C.-H. Lin, M. Asim, R. K. Yadav, M. Tariq, K. Satpathi, and B. Alamri, "A new high-gain DC-DC converter with continuous input current for DC microgrid applications," *Energies*, vol. 14, no. 9, p. 2629, May 2021.

[14] A. Ahmad, R. K. Singh, and A. R. Beig, "Switched-capacitor based modified extended high gain switched boost Z-source inverters," *IEEE Access*, vol. 7, pp. 179918–179928, 2019.

[15] L. Schmitz, D. C. Martins, and R. F. Coelho, "Comprehensive conception of high step-up DC–DC converters with coupled inductor and voltage multipliers techniques," *IEEE Trans. Circuits Syst. I, Reg. Papers*, vol. 67, no. 6, pp. 2140–2151, Jun. 2020.

[16] M. Forouzesh, Y. Shen, K. Yari, Y. P. Siwakoti, and F. Blaabjerg, "High-efficiency high step-up DC–DC converter with dual coupled inductors for grid-connected photovoltaic systems," *IEEE Trans. Power Electron*, vol. 33, no. 7, pp. 5967–5982, Jul. 2018.

[17] D. Bao, A. Kumar, X. Pan, X. Xiong, A. R. Beig, and S. K. Singh, "Switched inductor double switch high gain DC-DC converter for renewable applications," *IEEE Access*, vol. 9, pp. 14259–14270, 2021.

[18] M. Mohammadi, A. Dehbashi, G. B. Gharehpetian, A. Khoshsaadat, and P. Mattavelli, "A family of soft-switching DC–DC converters with two degrees of freedom," *IEEE Trans. Ind. Electron.*, vol. 68, no. 10, pp. 9398–9409, Oct. 2021.

[19] U. Rafiq, A. F. Murtaza, H. A. Sher, and D. Gandini, "Design and analysis of a novel high-gain DC-DC boost converter with low component count," *Electronics*, vol. 10, no. 15, p. 1761, Jul. 2021.

[20] A. M. S. S. Andrade, T. Faistel, R. A. Guisso, and A. Toebe, "Hybrid high voltage gain transformerless DC–DC converter," *IEEE Trans. Ind. Electron*, vol. 69, no. 3, pp. 2470–2479, Mar. 2021.

[21] Y. Ji, H. Liu, Y. Feng, F. Wu, and P. Wheeler, "High step-up Y-source coupled-inductor impedance network boost DC–DC converters with common ground and continuous input current," *IEEE J. Emerg. Sel. Topics Power Electron.*, vol. 8, no. 3, pp. 3174–3183, Sep. 2020.

[22] T. Nouri, N. Nouri, and N. Vosoughi, "A novel high step-up high efficiency interleaved DC–DC converter with coupled inductor and built-in transformer for renewable energy systems," *IEEE Trans. Ind. Electron.*, vol. 67, no. 8, pp. 6505–6516, Aug. 2019.

[23] Y. P. Siwakoti, P. C. Loh, F. Blaabjerg, S. J. Andreasen, and G. E. Town, "Y-source boost DC/DC converter for distributed generation," *IEEE Trans. Ind. Electron.*, vol. 62, no. 2, pp. 1059–1069, Feb. 2015.
[24] Y. Hu, J. Wu, W. Cao, W. Xiao, P. Li, S. J. Finney, and Y. Li, "Ultrahigh step-up DC–DC converter for distributed generation by three degrees of freedom approach," *IEEE Trans. Power Electron.*, vol. 31, no. 7, pp. 4930–4941, Jul. 2015.
[25] J. C. Rosas-Caro, F. Mancilla-David, J. C. Mayo-Maldonado, J. M. Gonzalez-Lopez, H. L. Torres-Espinosa, and J. E. Valdez-Resendiz, "A transformer-less high-gain boost converter with input current ripple cancelation at a selectable duty cycle," *IEEE Trans. Ind. Electron.*, vol. 60, no. 10, pp. 4492–4499, Oct. 2013.
[26] N. Genc and Y. Koc, "Experimental verification of an improved soft-switching cascade boost converter," *Electr. Power Syst. Res.*, vol. 149, pp. 1–9, Aug. 2017.
[27] Y.-M. Ye and K. W. E. Cheng, "Quadratic boost converter with low buffer capacitor stress," *IET Power Electron.*, vol. 7, no. 5, pp. 1162–1170, May 2014.
[28] K. Sayed, M. Abdel-Salam, A. Ahmed, and M. Ahmed, "New high voltage gain dual-boost DC-DC converter for photovoltaic power systems," *Electr. Power Compon. Syst.*, vol. 40, no. 7, pp. 711–728, Apr. 2012.
[29] S.-M. Chen, T.-J. Liang, L.-S. Yang, and J.-F. Chen, "A cascaded high step-up DC–DC converter with single switch for microsource applications," *IEEE Trans. Power Electron.*, vol. 26, no. 4, pp. 1146–1153, Apr. 2011.
[30] A. Al Nabulsi, M. Al Sabbagh, R. Dhaouadi, and H.-U. Rehman, "A 300 Watt cascaded boost converter design for solar energy systems," in *Proc. Int. Conf. Electr. Power Energy Convers. Syst. (EPECS)*, 2009, pp. 1–4.
[31] S.-W. Lee and H.-L. Do, "High step-up cascade synchronous boost DC–DC converter with zero-voltage switching," *IET Power Electron.*, vol. 11, no. 3, pp. 618–625, Mar. 2018.

R. V. DAMODARAN received the B.Tech. degree in electrical and electronics engineering from the Saintgits College of Engineering, Kerala, India, in 2014, and the M.Tech. degree in power and energy systems and the Ph.D. degree from the Department of Electrical and Electronics Engineering, National Institute of Technology, Karnataka, India, in 2017 and 2021, respectively. She is currently a Postdoctoral Fellow with the Department of Electrical Engineering, United Arab Emirates University, Al Ain, United Arab Emirates. Her research interests include the grid integration of solar PV systems, power conversion interfaces, and digital implementation of controls.

HUSSAIN SHAREEF (Member, IEEE) received the Ph.D. degree in electrical engineering from Universiti Teknologi Malaysia (UTM), Malaysia, in 2007. He is currently a Professor with the Department of Electrical Engineering, United Arab Emirates University. He is also the Head of the Green Mobility Research Team, Emirates Center for Mobility Research. He has published more than 400 peer-reviewed journal articles in various fields related to power and energy systems and has more than 5674 citations with an H-index of 37. His research interests include power system planning, integration of renewable power sources, application of AI techniques in power systems, energy management, power quality, and electric vehicle grid integration. He is a member of the Mohammed Bin Rashid Academy of Scientists. Among his many awards, he was a recipient of the UAE University Award for Excellence in Scholarship and the Chancellor Innovation Award (2020–2021). He appeared as the world's top 2% scientist by Stanford University, in 2019, 2020, and 2021.

K. S. PHANI KIRANMAI received the B.Tech. degree in electrical and electronics engineering from Sri Krishnadevaraya University, Andhra Pradesh, India, in 2001, and the M.E. degree in industrial drives and control from the Department of Electrical and Electronics Engineering, Osmania University, Hyderabad, India, in 2003. She is currently pursuing the Ph.D. degree with the Department of Electrical Engineering, United Arab Emirates University, Al Ain, United Arab Emirates. From 2003 to 2011, she worked as a research and development engineer in the solar PV industry. From 2012 to 2016, she was with solar PV power plant commissioning as a program manager. Her research interests include power electronics application and control in renewable energy conversion, control and management of energy storage systems, and thermal analysis of power electronic converters.

RACHID ERROUISSI (Senior Member, IEEE) received the Ph.D. degree in electrical engineering from the University of Quebec, Chicoutimi, QC, Canada, in 2010. From 2011 to 2014, he was a Postdoctoral Researcher with the Department of Electronics and Communication Engineering, University of New Brunswick. From 2014 to 2018, he was a Researcher/Teaching Associate with the Department of Electronics and Communication Engineering, Khalifa University, PI Campus, United Arab Emirates. Since January 2019, he has been an Assistant Professor with the Department of Electrical Engineering, United Arab Emirates University (UAEU). His research interests include advanced controls, disturbance observer approach, electric machines and drives, and renewable energy conversion systems. He is a registered Professional Engineer in the Province of New Brunswick, Canada.